Taylor & Francis
Taylor & Francis Group

Ship Technology Research
Schiffstechnik

ISSN: (Print) (Online) Journal homepage: www.tandfonline.com/journals/ystr20

First principle design load assessment of LH2 fuel gas supply systems for ships by means of 0D approach

Tobias Lampe, Bright E. Okpeke, Lukas Roß & Sören Ehlers

To cite this article: Tobias Lampe, Bright E. Okpeke, Lukas Roß & Sören Ehlers (27 Jan 2025): First principle design load assessment of LH2 fuel gas supply systems for ships by means of 0D approach, Ship Technology Research, DOI: 10.1080/09377255.2025.2452756

To link to this article: https://doi.org/10.1080/09377255.2025.2452756

Published online: 27 Jan 2025.

SHIP TECHNOLOGY RESEARCH (SCHIFFSTECHNIK)
https://doi.org/10.1080/09377255.2025.2452756

First principle design load assessment of LH2 fuel gas supply systems for ships by means of 0D approach

Tobias Lampe, Bright E. Okpeke, Lukas Roß and Sören Ehlers

German Aerospace Center (DLR), Institute of Maritime Energy Systems, Geesthacht, Germany

ABSTRACT

Within the framework of the Sustainable Development Goals, the United Nations (UN) General Assembly has declared its firm intention to combat climate change and the associated changes in the environment. Shipping is an important factor since its exhaust gases account for just over two per cent of global greenhouse gas (GHG) emissions. Liquid hydrogen is a promising candidate to enable this transition. In this work, a simulation-based approach for the estimation of design loads with respect to liquid hydrogen fuel tanks is presented. The MATLAB software was employed to implement a 0-dimensional approach for the calculation of the bulk thermodynamic behavior. There is good correlation between validation data and simulation. An exemplary cruise ship and corresponding power-demand profiles were utilized to simulate different fuel gas supply systems. The results were then analyzed with regard to occurring loads and operational efficiency.

ARTICLE HISTORY
Received 13 January 2023
Accepted 7 January 2025

KEYWORDS
Design loads; LH2; fuel gas supply system; fuel tank; superheated vapor model; 0D; thermodynamic behaviour

Nomenclature

$\dot{m}_{Tr}$ Transmission Line Mass Flow [kg s^{-1}]
$\dot{m}_F$ Cross-Film Mass Flow [kg s^{-1}]
$\dot{m}_R$ Relief Valve Mass Flow [kg s^{-1}]
$\dot{m}_C$ Compressor Mass Flow [kg s^{-1}]
$\dot{m}_{PBU}$ PBU Mass Flow [kg s^{-1}]
$\dot{m}_L$ Time Derivative of Liquid Mass [kg s^{-1}]
$\dot{m}_V$ Time Derivative of Vapor Mass [kg s^{-1}]
h_V Spec. Vapor Enthalpy [J kg^{-1}]
h_L Spec. Liquid Enthalpy [J kg^{-1}]
h_F Spec. Film Enthalpy [J kg^{-1}]
h_{Boil} Spec. Enthalpy of PBU Vapor [J kg^{-1}]
U_V Vapor Internal Energy [J]
U_L Liquid Internal Energy [J]
pdV Volume Work [J s^{-1}]
v Relief Flow Velocity [m s^{-1}]
$\dot{Q}_{EV}$ Heat Transfer Rate Environment to Vapor [J s^{-1}]
$\dot{Q}_{EL}$ Heat Transfer Rate Environment to Liquid [J s^{-1}]
$\dot{Q}_{VL}$ Heat Transfer Rate Vapor to Liquid [J s^{-1}]
$\dot{U}_V$ Time Derivative of Vapor Internal Energy [J s^{-1}]
$\dot{U}_L$ Time Derivative of Liquid Internal Energy [J s^{-1}]
T_L Liquid Temperature [K]
T_V Vapor Temperature [K]
T_V Environment Temperature [K]
T_F Film Temperature [K]
V_F Film Volume [m^3]
A_F Film Area [m^2]
A_L Area wetted by Liquid [m^2]
A_V Area covered by Vapor [m^2]
t_F Film Thickness [m]
c_{EL} Heat Transfer Coefficient Environment to Liquid [W m^{-2} K^{-1}]
c_{EV} Heat Transfer Coefficient Environment to Vapor [W m^{-2} K^{-1}]
c_{VL} Heat Transfer Coefficient Vapor to Liquid [W m^{-2} K^{-1}]
S_t State Vector []
$\dot{S}_t$ Time Derivative of State Vector []
ρ_L Liquid Density [kg m^{-3}]
ρ_V Vapor Density [kg m^{-3}]
f_e Evaporation Coefficient, 0.1
f_e Condensation Coefficient, 1

Introduction

Climate change presents an undisputed threat to the security and prosperity, as well as economic and social development, of the world as a whole. A major driving factor is greenhouse gas (GHG) emission. Human activities, namely, the burning of fossil fuels for electricity, heat and transportation, are almost exclusively responsible for the increase in GHG in the atmosphere over the last 150 years (Solomon et al. 2007). The United Nations (UN) General Assembly has therefore declared its firm intention to combat climate change and the associated changes in the environment within the framework of the Sustainable Development Goals (United Nations, G. A. 2022). Accordingly, similar

CONTACT Tobias Lampe tobias.lampe@dlr.de Düneberger Straße 108, 21502 Geesthacht, Germany

goals were adopted in the GHG Strategy of the International Maritime Organization (IMO), which intents to completely drive the maritime industry away from fossil fuels towards zero-carbon alternatives within this century (IMO 2018).

Hydrogen (H2) is a promising candidate to enable this transition. If H2 is produced using renewable energies, the net carbon dioxide (CO2) emissions are zero. In comparison with other alternative fuels, H2 has the additional benefit of being nontoxic. Nevertheless, certain disadvantages need to be considered, such as the high flammability of H2. Furthermore, due to its low energy density, space efficient storage of (liquid) H2 in a maritime context is only feasible at croygenic temperatures, thus creating highly demanding requirements for the utilized technologies, which have not been fully addressed yet. While other fuels subjected to cryogenic storage are already part of the IMO's International Code of Safety for Ship Using Gases or Other Low-flashpoint Fuels (IGF) (IMO 2015) and International Code of the Construction and Equipment of Ships Carrying Liquefied Gases in Bulk (IGC) (IMO 2016), class approval for liquid hydrogen (LH2) tanks and machinery is still based on the *alternative design approach*. Here, the applicant needs to provide an engineering analysis of the investigated system that shows that the alternative design and arrangements provide an equivalent level of safety compared to the prescriptive requirements. The approach should be based on sound science and engineering practice incorporating widely accepted methods, empirical data, calculations, correlations and computer models as contained in engineering textbooks and technical literature (IMO 2013). Although storage of H2 can also be facilitated by other means such as metal hydrides or e-fuels, the work presented by the authors focuses on cryogenic storage.

Due to inevitable heat ingress from the environment, the liquified gas contained in cryogenic storage tanks will exhibit evaporation of the contained liquified gas and thus lead to formation of co-existant vapor and liquid phases. Furthermore, heat transfer from vapor to liquid phase takes place since the vapor temperature is generally higher in comparison with the liquid (Kang et al. 2018; Hasan et al. 1991; Al Ghafri et al. 2022). The resulting temperature gradient within the liquid is termed thermal stratification. Depending on the modelling approach, the spatial resolution of this effect varies greatly. While 3D *Computational-Fluid-Dynamics* (CFD) simulations, which account for phase change, are available (Welch and Wilson 2000; Tryggvason and Lu 2015; Yang et al. 2008), the required computational effort renders usage of these methods infeasible in a design context. More suitable techniques consider basic conversation laws for the control volumes of vapor and liquid. Petitpas (2018) and Daigle et al. (2013) present methods, which provide a 1D and 2D assessment of stratification effects, respectively. For this purpose, additional control volumes, which further divide the computational domain, are introduced in both approaches. Since for initial design purposes, often only the thermodynamic behaviour of the bulk phases is of interest, many authors (Al Ghafri et al. 2022; Wang et al. 2020; Estey et al. 1983; Kalikatzarakis et al. 2022; Migliore 2016) employ a 0D model that does not account for spatial temperature gradients at all. Nevertheless, most modern approaches do not presume thermal equilibrium within the tank but allow superheating of the vapor. These methods are known as superheated vapor (SHV) models (Al Ghafri et al. 2022).

In this work, a simulation-based approach for the calculation of design loads, as well as tank specifications, for liquid hydrogen fuel tanks is presented. Making use of the MATLAB software, a 0D SHV method was implemented to assess the time-resolved thermodynamic behaviour. Since a 0D approach is utilized, the method is incapable of capturing quantitiy gradients within the respective phases. Furthermore, 3D effects such as fluid movement (sloshing) can not be resolved. Further research might address this issue by means of correction factors. The basic functionality of the method was validated by means of comparison with an experiment conducted at NASA's Lewis Research Center. To demonstrate the capabilities of the approach, three fuel gas supply systems (FGSS) consisting of the fuel tank and the respective appendages to enable fuel take-out and pressure control were investigated. Based on the power-demand profile of an exemplary cruise ship, suitable tank and isolation specifications were chosen, the corresponding fuel consumption was prescribed and the thermodynamic behaviour, as well as implications of tank design on operational efficiency, were analyzed. The current work advances the state of the art by addressing scenarios and systems specifically found in the maritime industry. This includes description of the respective FGSS and provision of suitable simplified modelling approaches, as well as usage of time resolved fuel demands obtained through measurements.

Method description

For the present work, key concepts detailed in the work of Petitpas (2018), Osipov and Muratov (2009) and Osipov et al. (2011), which establish the assumption of a thin, massless, saturated vapor film at the free surface between liquid and vapor, were adopted. Thus, the fuel tank is considered in terms of the three control volumes vapor phase, separation film and liquid phase. The liquid is assumed to be at saturation at

all times, while the vapor is allowed to superheat. The separation film is assumed to behave as saturated vapor. Contrary to the work of Petitpas (Petitpas 2018), any mass or energy flow is permitted to transition directly across the film into the other phase. Calculation of required thermodynamic properties is performed by means of the CoolProp package (Bell et al. 2014), which provides an implementation for the fundamental equations of state for parahydrogen, normal hydrogen and orthohydrogen based on the work of Leachman (Leachman et al. 2009). For the present publication, all tank contents are taken as pure parahydrogen.

Mass and energy balances

At basic, the method solves the mass and energy balances for the vapor and liquid control volumes, as depicted in Figure 1. For the mass balances, a transmission line flow $\dot{m}_{Tr}$ into or out of the liquid phase, an evaporation or condensation flow through the film $\dot{m}_F$, a relief flow through a vent valve $\dot{m}_R$, a compressor flow out of the vapor phase $\dot{m}_C$, as well as a pressure build-up unit (PBU) flow $\dot{m}_{PBU}$, are taken into account. The PBU evaporates LH2 and pressurizes the tank by feeding the evaporated gas into the vapor phase and it is assumed to operate without time delay and at 100% efficiency, such that all evaporated liquid is immediately transferred to the vapor phase.

With regard to the energy balances, the enthalpies associated with the mass flows are considered. Variables h_V, h_L, h_F and h_{Boil} denote the enthalpies of vapor, liquid, film and vapor output from the PBU. Here and in the following, subscripts V, L, F and E will denote vapor, liquid, film and environment. In case of the relief valve flow, the kinetic energy is taken into account via the relief valve flow velocity v, which is neglected for all other mass flows. For both vapor and liquid phase, the work due to volume changes pdV is considered. Finally, the heat transfers from environment to vapor $\dot{Q}_{EV}$, from environment to liquid $\dot{Q}_{EL}$, as well as from vapor to liquid $\dot{Q}_{VL}$, are accounted for.

Based on these considerations, the vapor and liquid mass balances are taken as

$$\dot{m}_V = \dot{m}_F - \dot{m}_R - \dot{m}_C + \dot{m}_{PBU} \tag{1}$$

and

$$\dot{m}_L = -\dot{m}_{Tr} - \dot{m}_F - \dot{m}_{PBU}, \tag{2}$$

with $\dot{m}_V$ and $\dot{m}_L$ as the time derivatives in overall vapor and liquid mass, respectively. The energy balances read as

$$\dot{U}_V = \dot{Q}_{EV} - \dot{Q}_{VL} - pdV - \dot{m}_R(h_V + 0.5v^2) + \dot{m}_F h_F - \dot{m}_C h_V + \dot{m}_{PBU} h_{boil} - \dot{m}_V u_V \tag{3}$$

and

$$\dot{U}_L = \dot{Q}_{EL} + \dot{Q}_{VL} + pdV - \dot{m}_{Tr} h_L - \dot{m}_F h_F - \dot{m}_{PBU} h_L - \dot{m}_L u_L, \tag{4}$$

with v as the velocity of the relief valve flow. Here, $\dot{U}_V$ and $\dot{U}_L$ denote the time derivatives of vapor and liquid internal energy, while u_V and u_L denote the mass

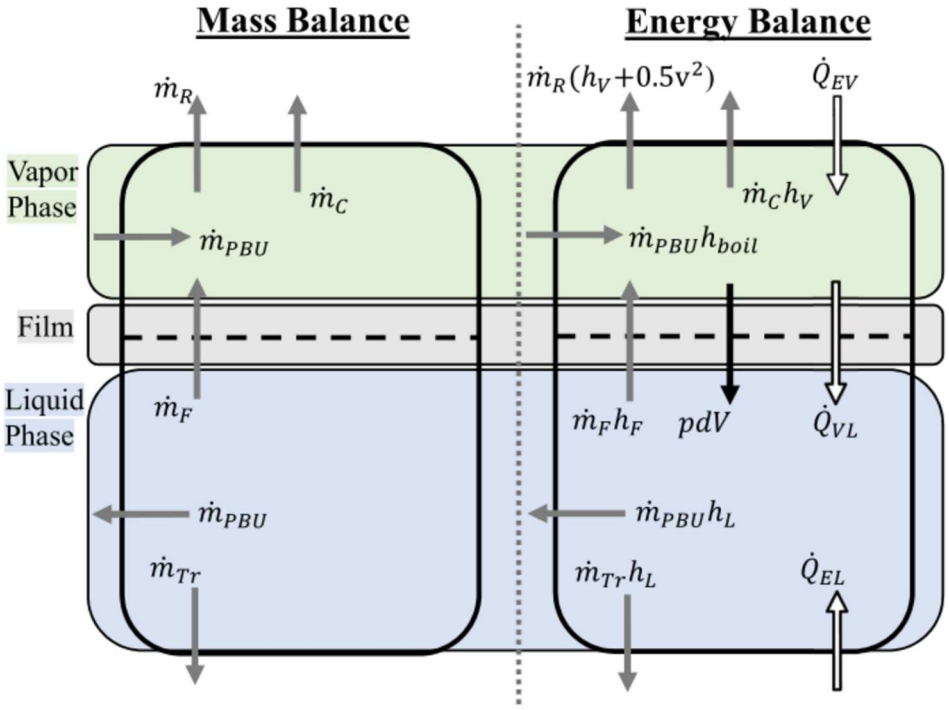

Figure 1. Mass and energy balances.

specific internal energy of vapor and liquid, respectively.

Calculation of required values

In the following, the acquisition of the various terms needed to set up the mass and energy balances is described. The transimission, PBU and compressor mass flows are assumed to be known. While the relief valve mass flow is calculated based on the ambient and tank pressures and the valve orifice area, the exact formulas (OSTI.GOV 1993) are omitted for the sake of brevity. Following a variation of the Lee Model (Lee 2013) reported by Yang et al. (2008), the mass flow across the separation film is modelled as

$$\dot{m}_F = f_e V_F \rho_L (T_L - T_F)/T_F, \tag{5}$$

for $T_L \geq T_F$, otherwise

$$\dot{m}_F = -f_c V_F \rho_V (T_L - T_F)/T_F \tag{6}$$

holds. In this case, ρ indicates density while T refers to the respective temperatures and V_F is the film volume. The film volume is given by

$$V_F = t_F A_F. \tag{7}$$

To acquire the film volume, the film cross section area A_F is calculated based on tank geometry and fill level while the film thickness is, based on experimental work (Beduz and Scurlock 1994), simply assumed as $t_F = 0.005m$. The constants f_e and f_c are associated with evaporation and condensation. For the calculations $f_e = 0.1$ and $f_c = 1$ are used.

The enthalpy of the transmission flow and the flow from liquid phase to PBU are obtained according to the current (saturated) thermodynamic state of the liquid. For the separation film flow an enthalpy equal to that of saturated vapor is assumed. In case of the relief valve and compressor flow, the actual thermodynamic state of the vapor is considered. With regard to the vapor input from PBU to the tank, dry saturated vapor at a given temperature is assumed to acquire the corresponding enthalpy. The heat ingress from environment to vapor and environment to liquid is computed according to

$$\dot{Q}_{EV} = c_{EV} A_V (T_E - T_V) \tag{8}$$

and

$$\dot{Q}_{EL} = c_{EL} A_L (T_E - T_L), \tag{9}$$

respectively, with c_{EV} and c_{EL} as the heat transfer coefficients and A_V and A_L as the respective contact areas. Similarly, the heat transfer from vapor to liquid is calculated as

$$\dot{Q}_{VL} = c_{VL} A_F (T_V - T_L). \tag{10}$$

The coefficient c_{VL} can either be prescribed or obtained based on Rayleigh and Nusselt numbers under the assumption of heat transfer for the bottom surface of a hot plate (Böckh and Wetzel 2014).

Solution algorithm

To simulate the time-resolved thermodynamic behaviour, Equations (1)–(4) are integrated into a solution algorithm, as illustrated in Figure 2. At the beginning of each time step, the state vector S_t, which contains liquid and vapor mass, as well as internal energy of liquid and vapor, needs to be known. At the start of the simulation, the vector is defined according to the initial conditions. Assuming saturation, liquid density and temperature are obtained based on the liquid's specific internal energy. CoolProp does not allow usage of specific internal energy as input to acquire saturation properties, and therefore polynomials relating internal energy and the respective quantities are used instead. As the state vector contains the liquid mass, the liquid volume can be computed. Utilizing simple equations and knowledge of the overall tank volume, vapor volume and accordingly vapor density are calculated. With this, two intensive properties of the vapor are known, and vapor pressure and temperature are acquired via CoolProp. Since the separation film is assumed to behave as saturated vapor, the film temperature is given by either of the vapor's intensive properties. To set up and solve the mass and energy balances, the required values are calculated based on the considerations given previously. Resulting from the balance equations, the time derivative of the state vector $\dot{S}_t$ for the current time step is acquired. This derivative is then passed to MATLAB's ODE15s solver to acquire the state vector of the next time step. The process is repeated until the specified

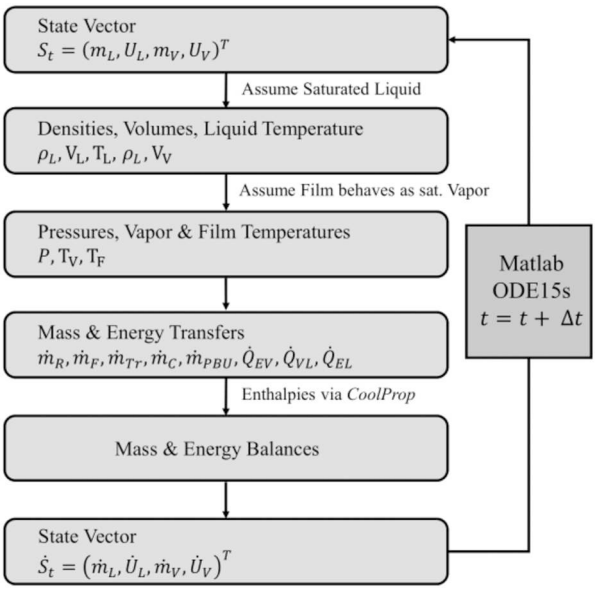

Figure 2. Solution algorithm.

simulation end time is reached. Apart from the variables used in the solution process, any thermodynamic quantities available through CoolProp can be computed and recorded within the simulation.

Validation and verification

Validation data for fuel tank systems, including the supply system and pressure control components, such as relief valve, PBU and compressor, is,unfortunately, not readily available in literature. Validation was therefore performed by means of comparison of simulation results with a self-pressurization experiment (Hasan et al. 1991) conducted at the NASA Lewis Research Center's K-Site Facility. In the experiment, an ellipsoidal tank is filled with LH2. Tank venting is then maintained until steady boil-off starting conditions are present. In the following, pressure and temperatures in the tank are measured. While Hasan et al. (1991) report the required tank parameters and initial conditions for the simulations, the heat ingress is described by means of an average heat flux $Q = 3.5\,\mathrm{W\,m^{-2}}$. In the current approach, the heat transfer coefficients (see Equations (8)–(10)) are needed, which were prescribed according to the values used by Al Ghafri et al. (2022) who also employ the experiment for validation purposes and acquire the coefficients based on measured experimental heat fluxes (Equations (8), (9)) and optimal capturing of the results (Equation (10)). Accordingly, the focus of the validation case is to demonstrate that the thermodynamic interplay within the tank is captured correctly. Since the respective coefficients are usually not known a priori, for simulations beside the validation case they are calculated based on standard formulas (Böckh and Wetzel 2014). For the heat transfer between vapor and liquid, the modelling approach is, as commonly utilized in literature (Kalikatzarakis et al. 2022; Migliore 2016; Wang et al. 2020), based on the assumption of convective heat transfer of a plate with uniform temperature. For the heat transfer from the environment to the respective phase, the coefficients are acquired based on insulation material and thickness. The tank was modelled as a spherical geometry with the same volume as the tank in the experiments. A summary of the simulation parameters, as well as the initial conditions, is found in Table 1. MATLAB's ODE15s solver determines the best time step size on its own, therefore only a maximum value is provided. A comparison of simulation results and measured pressures is given in Figure 3, which shows good agreement between both. Due to the heat ingress from the environment, liquid is evaporated, which causes, together with the increase in temperature, an increase in tank pressure. While the current method's estimation of pressure in the first four hours is slightly different from the experiment, overall trends and especially the rate of change in the remaining time are captured very well. The same holds true for the results concerning vapor and liquid temperatures, as depicted in Figure 4. Throughout the simulation, the relative error between simulation and experiment reaches a maximum of 3%, 2.37% and 1.69% for pressure, vapor temperature and liquid temperature, respectively. As a result of the heat transfer from the environment, liquid and vapor experience an increase in temperature. Due its different thermodynamic properties, the effect is more pronounced for the vapor. In the experiment, temperatures are measured at different locations in the tank. The computed vapor temperature is compared to the uppermost and therefore fully emerged sensor. For comparison with the computed liquid temperatures, the sensor, which is submerged but closest to the liquid surface, was chosen as Hasan et al. (1991) report saturation conditions in the vicinity of the liquid surface. There is good agreement between simulation and experiments regarding qualitative and quantitative

Table 1. Validation case setup.

Variable	Description	Value	Unit
V_S	Sphere Volume	4.89	m^3
	Initial Fill Level	83	%
P_{ini}	Initial Pressure	105	kPa
$T_{L,ini}$	Initial Liquid Temp.	20.4	K
$T_{V,ini}$	Initial Vapor Temp.	20.4	K
T_E	Environment Temperature	350	K
c_{VL}	Heat Transfer Vapor to Liquid	1.04	$W\,m^{-2}\,K^{-1}$
c_{EL}	Heat Transfer Environment to Liquid	0.0351	$W\,m^{-2}\,K^{-1}$
c_{EV}	Heat Transfer Environment to Vapor	0.0351	$W\,m^{-2}\,K^{-1}$
t_{end}	Simulation End Time	14	h
Δt_{max}	Maximum Time Step	120	s

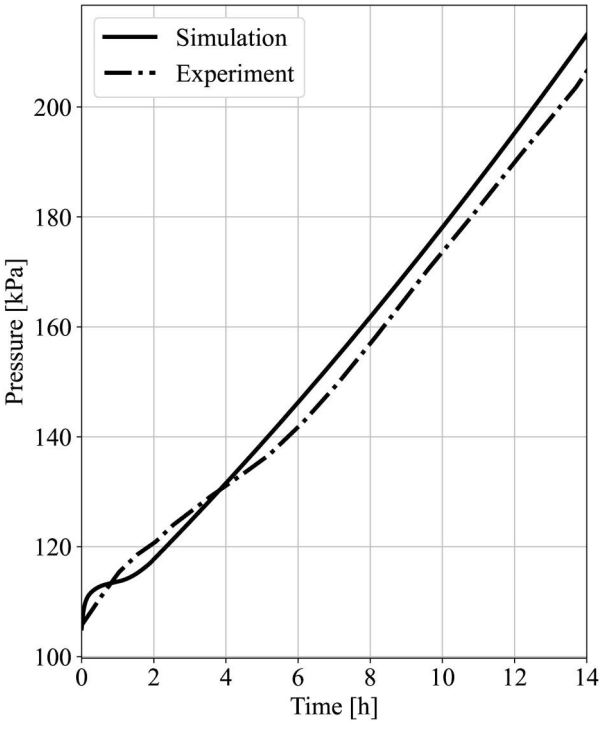

Figure 3. Calculated and measured time history of pressure.

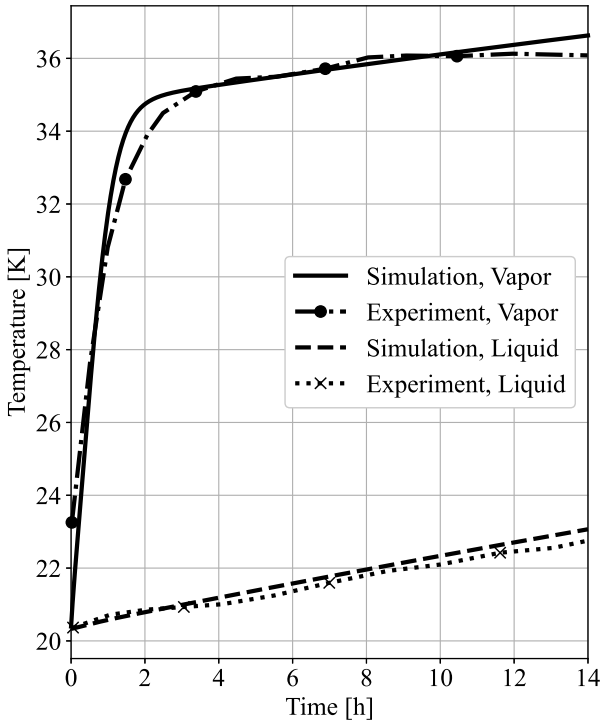

Figure 4. Calculated and measured time history of vapor and liquid temperature.

behavior. Stratification effects, which are not captured by the current model, do take place in the experiment. The temperatures at the liquid surface and close to the tank bottom differ by about 1 K. To justify the choice of $f_e = 0.1$ and $f_c = 1$, see Equations (5) and (6), calculations, in which the respective constants were varied, were carried out. Figure 5 presents the time history of

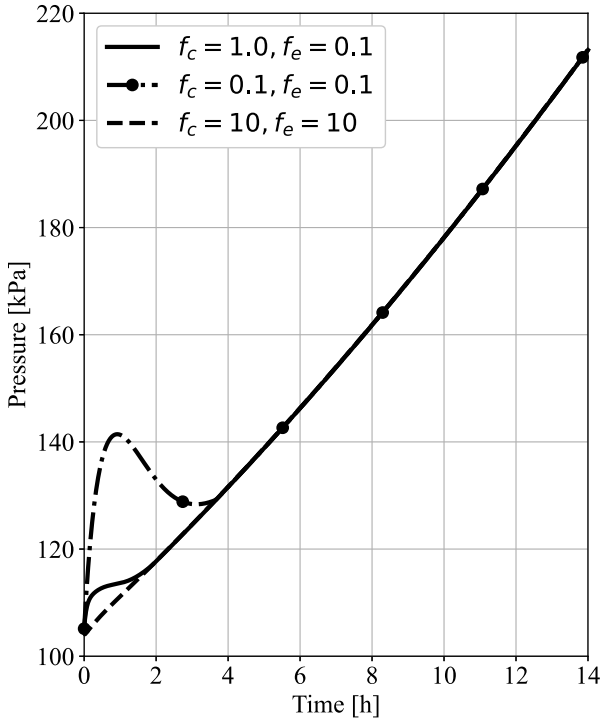

Figure 5. Calculated time history of pressure for varying evaporation and condensation constants.

pressure for three value combinations. While the choice of the constants affects the pressure behaviour in the initial stage, there is practically no influence afterwards. The same is observed for other quantities such as vapor temperature, liquid temperature and boil-off. Table 2 presents the values of exemplary quantities at the end of the simulation. Wang et al. (2020) report similar findings, stating that only very high and low values of f_e and f_c lead to the numerical divergence and underestimating the pressure rise, respectively. The choice of the constants in this work was motivated by favourable agreement with the experimental data at the early stage of the simulation.

Assessment framework

Different aspects of fuel tank and FGSS design were investigated. Based on a given fuel demand, suitable tank sizes were estimated and the thermodynamic behaviour was analyzed considering different configurations. The utilized FGSS concepts are illustrated in Figure 6(a–c). In *FGSS 1*, a given pressure is maintained in the tank by means of a PBU. The pressure value needs to be adjusted considering the minimum working pressure of the FGSS since fuel take-out is simply realized by opening the transmission line valve. It is assumed that the control strategy for the transmission valve is perfect, such that the requested fuel demand is exactly met at all times. The PBU is assumed to deliver nominal in- and output mass flows immediately upon activation and is operated with a simple on/off control strategy with regard to given minimum and maximum pressure values. Unrestricted pressure increase in the tank is prevented by means of a relief valve, which is present in all FGSS variants. In case of *FGSS 2*, fuel take-out is managed by a wet sump pump. The control strategy for the pump is assumed to be perfect, such that the requested fuel demand is exactly met at all times. This infers that the pump is simply modelled by manipulation of the mass flow through the transmission line. Except for the relief valve, no additional pressure control systems are utilized. *FGSS 3* consists of the system denoted as *FGSS 2*, with an additional compressor for pressure control. The compressor is operated with a simple on/off control strategy. As soon as a given maximum pressure would be reached, the compressor is activated and operates at nominal mass flow until the pressure would fall below a given minimum value. In all FGSS variants the fuel taken out is LH2, which was assumed to be evaporated in subsequent components before being supplied to the actual consumer. The compressor in *FGSS 3* is an exception since in an actual system the vapor output would not be vented but also supplied to the consumer. Consequently, the fuel demand of the consumer would already be satisfied to an extent, decreasing the required flow

Table 2. Values at end of simulation for varying condensation and evaporation constants.

Variable	$f_c = 1.0, f_e = 0.1$	$f_c = 0.1, f_e = 0.1$	$f_c = 10, f_e = 10$
Liquid Temperature [*K*]	23.066	23.066	23.066
Vapor Temperature [*K*]	36.628	36.628	36.628
Vapor Mass [*kg*]	0.922	0.922	0.922

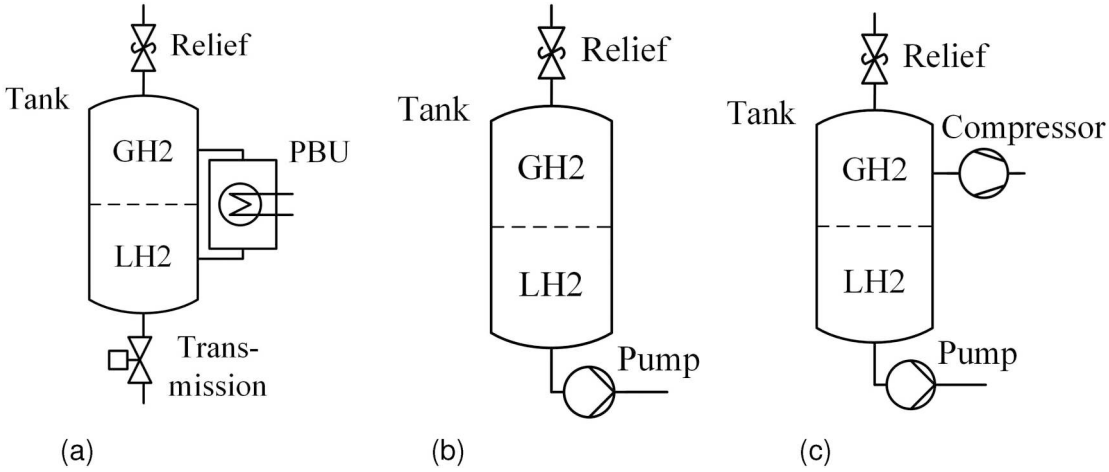

Figure 6. FGSS concepts. (a) FGSS 1 setup. (b) FGSS 2 setup and (c) FGSS 3 setup.

enabled by the wet sump pump. This effect is currently neglected in the method. Also, modelling of subsequent components such as a heater for the output flow of the compressor is not performed in this work since the focus lies on the thermodynamic behaviour in the tank.

To provide a realistic estimation of the fuel demand, the power demand profile of an exemplary cruise ship investigated by Baldi et al. (2018) was utilized. The reported power demand over the course of a typical day of operation was transformed to fuel demand mass flow assuming a heating value of 120 MJ kg^{-1} and a conversion efficiency of $\eta = 0.5$, see Figure 7. The tank geometry was taken as a horizontal cylinder with flat ends. Based on these premises and the specifications reported in Table 3, simulations were performed for different FGSS concepts and analyzed considering physical consistency. As the investigated ship is 176.9 m long and has a beam of 28.6 m, integration of a tank sized for operation with LH2 is deemed a challenging but not impossible task. After presentation of the results for the individual supply systems, a comparative study is shown for different combinations of tank size, insulation parameters and FGSS concepts. In this case, it was assumed that the ship performs consecutive days of operation until refuelling is needed with instantaneous jumps in demand at intersections between days.

Results

In the following, results for different FGSS setups are shown. General simulation parameters for the exemplary cases involving different fuel gas supply systems are given in Table 3. At the start of the simulations, saturation conditions and thermal equilibrium between vapor and liquid phase were assumed. Transfer coefficients for heat ingress from environment to each phase werecalculated based on standard formulas (Böckh and Wetzel 2014) considering the given parameters for insulation thickness and conductivity.

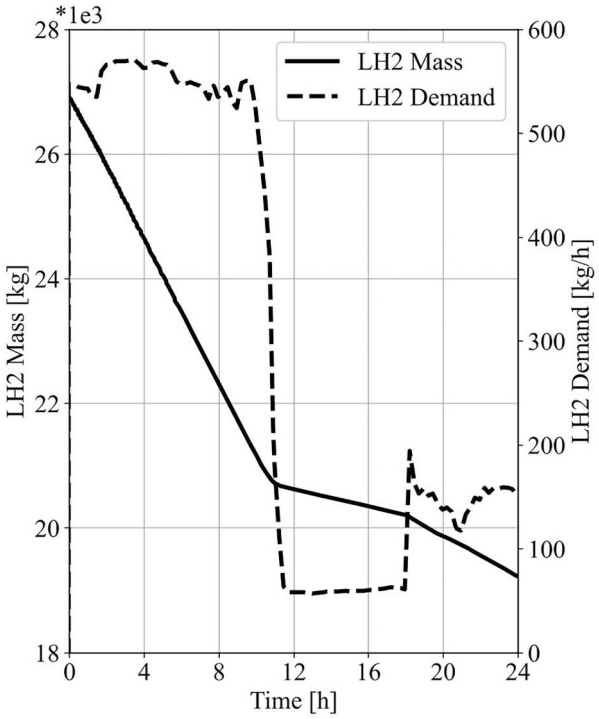

Figure 7. Liquid mass and fuel demand time history for FGSS 1.

Table 3. General simulation parameters.

Variable	Description	Value	Unit
V_C	Cylinder Volume	450	m^3
r_C	Cylinder Radius	2.5	m
L_C	Cylinder Length	22.91	m
	Initial Fill Level	85	%
P_{ini}	Initial Pressure	100	kPa
T_E	Environment Temperature	300	K
s	Insulation Thickness	1	m
k	Insulation Conductivity	0.04	$W\,m^{-1}\,K^{-1}$
t_{end}	Simulation End Time	24	h
Δt_{max}	Maximum Time Step	120	s

Table 4. PBU parameters.

Variable	Description	Value	Unit
$\dot{m}_{PBU}$	Mass Flow	0.3	$kg\,s^{-1}$
$P_{PBU,min}$	Min. Control Pressure	350	kPa
$P_{PBU,max}$	Max. Control Pressure	400	kPa
T_{boil}	Recirc. Vapor Temp.	22	K
h_{boil}	Recirc. Vapor Enthalpy	454.2	$kJ\,kg^{-1}$

The thermal conductivity was taken based on values commonly assumed for perlite. For the chosen insulation, a maximum boil-off gas (BOG) rate of 0.1% per day during a 24 hour holding period was predicted. As BOG rates of 0.6% or less have been reported for very large tanks (Godula-Jopek et al. 2012), this prediction seems reasonable. The transfer coefficient for heat ingress from vapor to liquid was continuously re-calculated during the simulations based on Rayleigh and Nusselt numbers associated with convective heat transfer of a flat plate.

FGSS 1

The *FGSS 1* setup involves usage of a PBU to establish the required working pressure of the system, which for this case is specified as 350 kPa. A summary of the PBU parameters is provided in Table 4. As *FGSS 1* requires pressurization of the tank to working pressure before fuel supply is possible, simulations were conducted for the pressurization period and the operation period of 24 hours. Furthering accessibility of the data, results are only reported for the operation period. Figure 7 presents the development of LH2 mass in the tank along with the LH2 demand of the ship. The liquid mass is depleted at the highest pace during the first 10 hours of the simulation, which matches with the corresponding high level in fuel demand. Afterwards, a period of moderate depletion and demand follows, which slightly increases after about 18 hours. For this case, the filling level of the tank reaches a value of about 70% after a single day of operation, thus allowing for further usage without refuelling. The behaviour of pressure as well as temperature of liquid and vapor, over time, is given in Figure 8. In this case, a logarithmic scale was chosen for the time axis to preserve visual resolution of the oscillations. Due to the outflow of liquid mass, usage of the PBU is required for about 6 hours to maintain working pressure, resulting in oscillations of tank pressure (see Figure 8(a)) in between the specified interval from 350 kPa to 400 kPa. After the first six hours, the PBU does not activate any more since a state has been reached in which the combined influence of temperature rise and evaporation of LH2 leads to a continuous increase in tank pressure despite the mass outflow. The vapor temperature, along with the liquid temperature, is shown in Figure 8(b). In general, an average temperature increase of about 4 K is observed during the simulation. Although the PBU imposes mass flows on both vapor and liquid phase, oscillations in temperature are very distinct for the vapor and miniscule for the liquid. The reasons for this are twofold. The PBU mass inflow to the vapor

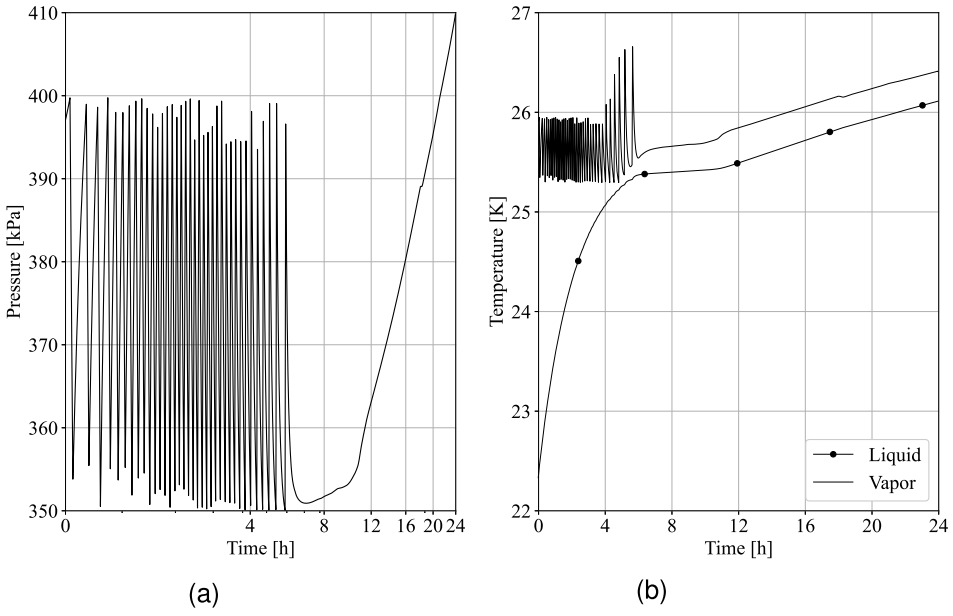

Figure 8. Pressure and temperature time history for FGSS 1 setup. (a) Pressure and (b) Temperatures.

Table 5. Relief valve parameters.

Variable	Description	Value	Unit
d_R	Orifice Diameter	0.008	m
$P_{R,min}$	Lower Valve Control Pressure	140	kPa
$P_{R,\max}$	Upper Valve Control Pressure	150	kPa

Table 6. Compressor parameters.

Variable	Description	Value	Unit
$\dot{m}_C$	Mass Flow	0.04	kg s^{-1}
$P_{C,min}$	Min. Pressure	120	kPa
$P_{C,\max}$	Max. Pressure	130	kPa

phase changes the vapor density. Furthermore, the thermodynamic properties of the inflow are governed by the PBU and are therefore different from the present vapor state, thus inciting the changes in vapor temperature. As the liquid phase is only subjected to mass outflow and kinetic effects are disregarded, the effect of PBU usage on the thermodynamic state of the liquid is found almost solely in the altered heat and mass flows in between both phases. The influence of decreased liquid mass is negligible considering the PBU mass flow is small in comparison to the bulk mass of the liquid.

FGSS 2

The *FGSS 2* setup makes use of a wet sump pump to establish fuel supply. It is therefore not needed to increase tank pressure by means of a PBU and fuel can be supplied without prior measures. Simulations were therefore conducted only for the operation period. Excessive tank pressure is prevented by means of a relief valve, for which the specifications are given in Table 5. Simulation results for pressure and temperatures in the tank are depicted in Figure 9. Although the volume available for the vapor phase increases due to outflow of LH2 through the transmission line, the pressure continuously rises due to temperature rise and evaporation of liquid, except for a small initial drop (see Figure 9(a)). At about 22 hours, the maximum pressure setting of the relief valve is reached. The valve is then opened, causing vapor outflow and a corresponding drop in pressure to the minimum pressure setting. At this point, the valve is closed and the pressure starts to rise again. For the remaining part of the simulation, the pressure oscillates in between the control values specified for the relief valve in accordance with the alternating valve status. Figure 9(b) shows the behaviour of liquid and vapor temperature over time. At the start of the simulation, thermal equilibrium is present, followed by a sharp rise in vapor temperature. After the initial rise, the vapor temperature continuously increases until the relief valve is opened, which in turn causes a temperature drop. In the following, the vapor temperature displays an oscillatory behaviour due to operation of the relief valve. Except for the initial rise, the liquid temperature behaves highly similar. After a period of continuous increase, oscillations take place after the relief valve starts operating.

FGSS 3

Similar to the previous setup, the *FGSS 3* setup makes use of a wet sump pump to establish fuel supply. Apart from the relief valve, this setup utilizes a compressor for pressure control, thus offering the possibility to restrict pressure to a specified value. The compressor parameters used for the simulations are given in Table 6. Simulation results for pressure and temperature obtained for the *FGSS 3* case are made

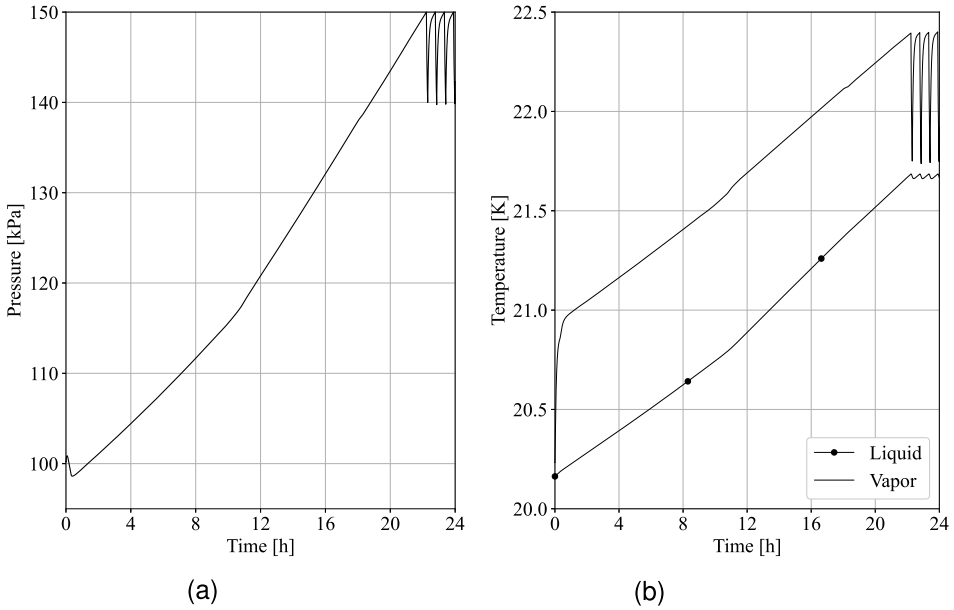

Figure 9. Pressure and temperature time history for FGSS 2 setup. (a) Pressure and (b) Temperatures.

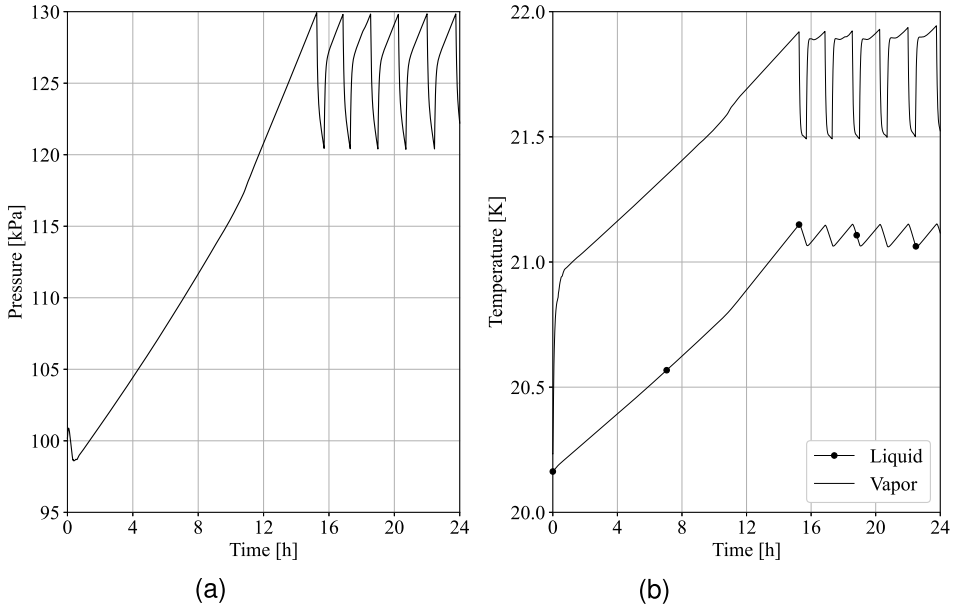

Figure 10. Pressure and temperature time history for FGSS 3 setup. (a) Pressure and (b) Temperatures.

available in Figure 10. Before usage of the compressor starts at about 15 hours, the behaviour of pressure and temperature is identical to the *FGSS 2* case. Since the processes of vapor release by relief valve and vapor extraction by compressor are similar, the temporal progress observed in the following is also alike. As soon as the pressure (see Figure 10(a)) reaches the specified maximum pressure control value of the compressor, vapor is extracted from the tank, thus causing the pressure to drop until the minimum pressure value is almost reached. At this point operation of the compressor is halted, causing the pressure to rise again until the maximum control value. These oscillations continue until simulation end. Likewise, the temperature of vapor and liquid (see Figure 10(b)) rise until first activation of the compressor, which causes a drop in temperature. In the following, oscillations in both vapor and liquid temperature take place in accordance with the operation status of the compressor.

Comparison of different FGSS setups

For each of the presented FGSS setups, simulations of a cylindric tank geometry with varying volume and insulation thickness were conducted. The transmission line flow was defined by the LH2 demand depicted in Figure 7. Initial pressure, fill level and environment temperature are given in Table 3 while the specifications for vaporizer and compressor can be found in Tables 4 and 6, respectively. The relief valve parameters werechosen such that the valve does not open during the simulation, as it was assumed the tank is designed to withstand the occurring pressures during normal operation. Furthermore, it was assumed that the liquid mass in the tank is not allowed to drop below 20% of the initial liquid mass. The simulations were run until this value was reached. Table 7 summarizes selected results from the simulations. Addtionally, results for 24 hour pure boil-off cases, denoted by '–', are included for comparison. For each case, the FGSS setup, tank volume V_C and insulation thickness s are reported along with the resulting maximum pressure $P_{\max}$, maximum vapor temperature $T_{V,\max}$, BOG per day percentage and simulation end time t_{end}. BOG percentages were taken with respect to initial liquid mass. For the *FGSS 1* configuration, liquid evaporated by the PBU was considered as BOG. Comparing the pure boil-off cases to those that involve fuel take-out it is apparent that the BOG percentage increases by a large margin, reaching values exceeding 10 % per day in particular cases, see e.g. the results for FGSS 3. Since this behaviour is related to the inclusion of additional components such as pumps and compressors, which have not been validated, in the simulation, the associated error margin is of interest. Considering the components were modelled using highly simplifying

Table 7. Results for different FGSS setups, tank sizes and insulations.

FGSS	V_C [m^3]	s [m]	$P_{\max}$ [kPa]	$T_{V,\max}$ [K]	BOG[%/day]	t_{end} [h]
–	200	1	–	–	0.079	24
–	450	1	–	–	0.072	24
1	200	1	412.8	28.26	4.89	28.25
1	200	0.25	716.33	29.95	9.12	27.29
1	450	1	476.2	27.24	2.84	58.76
1	450	0.25	1046.37	31.84	7.24	54.12
2	200	1	171.12	23.28	2.1	27.72
2	200	0.25	509.23	28.48	6.42	26.73
2	450	1	276.9	25.037	1.59	60.49
2	450	0.25	869.9	30.88	5.87	54.33
3	200	1	129.99	22.46	2.91	27.53
3	200	0.25	129.99	24.93	12.02	25.52
3	450	1	129.99	22.42	2.98	57.43
3	450	0.25	129.99	24.696	11.59	49.26

assumptions for thermodynamic behaviour and control strategies, it is expected that the results are qualitatively correct but not of high fidelity. Concerning the tank sizes, a larger tank will, provided FGSS setup and insulation are the same, always yield lower BOG percentages when compared with a smaller tank, as the surface to volume ratio is more favourable. With regard to the FGSS setups, *FGSS 2*, which is conceptually most similar to pure boil-off cases, shows the lowest BOG percentages while *FGSS 3* displays the largest evaporation of fuel. Pressurization of the tank via PBU and pressure control via compressor both further increase the amount of boil-off. With regard to the occurring pressures, *FGSS 3* is most favourable as the pressure is limited according to the compressor control values. As it involves pressurization of the tank prior to operation, *FGSS 1* displays the highest pressures. Similar findings are observed for the vapor temperature.

Conclusion

In this work, a method suitable for the design of fuel tanks housing cryogenic substances was presented. A 0D SHV method was implemented that considers vapor and liquid as individual phases with heat transfer between each other, as well as separate heat ingress from the environment. Validation of the method with regard to pure boil-off cases shows highly promising results, capturing overall trends and quantitative behaviour with good accuracy. Thus, the method was employed to simulate three fuel gas supply systems commonly used in maritime applications, yielding physically consistent results. Unforunately, measurement data for these configurations is not readily available. Further work should target validation of the method by means of more complex system including appending components. Nevertheless, the model can serve as a helpful tool to assess the complex interplay of compliance with regulations, investment and operation that needs to be considered in upcoming challenges regarding fuel tank design. As an example, a case study investigating the influence of basic tank parameters on occurring loads and fuel loss due to evaporation was performed. Further work will address the influence of currently neglected effects such as sloshing, as well as experiments and measurements regarding the behaviour of the presented supply sytem configurations.

Acknowledgments

The authors would like to thank Guillaume Petitpas for making his LH2 simulation code publicly available. The code provided the key ideas for the present method, in particular the structure of the solution algorithm and balance equations for the pure boil-off case.

Disclosure statement

No potential conflict of interest was reported by the author(s).

ORCID

Tobias Lampe http://orcid.org/0000-0002-8947-7379
Bright E. Okpeke http://orcid.org/0009-0006-9277-9681
Lukas Roß http://orcid.org/0000-0002-1641-9469
Sören Ehlers http://orcid.org/0000-0001-5698-9354

References

Al Ghafri S, Swanger A, Jusko V, Siahvashi A, Perez F, Johns M, May E. 2022. Modelling of liquid hydrogen boil-off. Energies. 15:1149. doi: 10.3390/en15031149

Baldi F, Ahlgren F, Nguyen T-V, Thern M, Andersson K. 2018. Energy and exergy analysis of a cruise ship. Energies. 11(10):2508. doi: 10.3390/en11102508

Beduz C, Scurlock RG. 1994. Evaporation mechanisms and instabilities in cryogenic liquids. In: Kittel P, editor. Advances in cryogenic engineering. Boston (MA): Springer US; p. 1749–1757.

Bell I, Wronski J, Quoilin S, Lemort V. 2014. Pure and pseudo-pure fluid thermophysical property evaluation and the open-source thermophysical property library CoolProp. Ind Eng Chem Res. 53(6):2498–2508. doi: 10.1021/ie4033999

Böckh P, Wetzel T (2014). Wärmeäbertragung – Grundlagen und Praxis. Heidelberg: Springer Vieweg Berlin.

Daigle M, Boschee J, Foygel M, Smelyanskiy V. 2013. Temperature stratification in a cryogenic fuel tank. J Thermophys Heat Transf. 27(2):116–126. doi: 10.2514/1.T3933

Estey P, Lewis D, Connor M. 1983. Prediction of a propellant tank pressure history using state space methods. J Spacecr Rockets. 20:49–54. doi: 10.2514/3.28355

Godula-Jopek A, Jehle W, Wellnitz J (2012). Hydrogen storage technologies: new materials, transport, and infrastructure. Wiley.

Hasan M, Lin C, Vandresar N. 1991. Self-pressurization of a flightweight liquid hydrogen storage tank subjected to low heat flux. In: Proceedings of the ASME/AIChE National Heat Transfer Conferen.

IMO. 2013. Guidelines for the approval of alternatives and equivalents as provided for in various IMO instruments. In: MSC.1/Circ.1455. London: International Maritime Organization.

IMO. 2015. International code of safety for ship using gases or other low-flashpoint fuels (IGF code). London: International Maritime Organization.

IMO. 2016. International code for the construction and equipment of ships carrying liquefied gases in bulk (IGC code). London: International Maritime Organization.

IMO. 2018. Adoption of the initial IMO strategy on reduction of GHG emissions from ships and existing IMO activity related to reducing GHG emissions in the sipping sector. In: MEPC.304(72), Talanoa dialogue. London: International Maritime Organization.

Kalikatzarakis M, Theotokatos G, Coraddu A, Sayan P, Yew Wong S. 2022. Model based analysis of the boil-off gas management and control for LNG fuelled

vessels. Energy. 251:123872. doi: 10.1016/j.energy.2022.123872

Kang M, Kim J, You H, Chang D. 2018. Experimental investigation of thermal stratification in cryogenic tanks. Exp Therm Fluid Sci. 96:371–382. doi: 10.1016/j.expthermflusci.2017.12.017

Leachman J, Jacobsen R, Penoncello S, Lemmon E. 2009. Fundamental equations of state for parahydrogen, normal hydrogen, and orthohydrogen. J Phys Chem Ref Data. 38:09. doi: 10.1063/1.3160306

Lee W. 2013. A pressure iteration scheme for two-phase flow modeling. In: Computational methods for two-phase flow and particle transport. https://www.perlego.com/book/847394/computational-methods-for-twophase-flow-and-particle-transport-pdf

Migliore C. 2016. Modelling the weathering process of stored liquefied natural gas (LNG) [PhD thesis]. London, UK: Imperial College of London.

Osipov V, Muratov B. 2009. Dynamic condensation blocking in cryogenic refueling. Appl Phys Lett. 93:224105–224105. doi: 10.1063/1.3025674

Osipov V, Daigle J, Muratov B, Foygel M, Smelyanskiy N, Watson D. 2011. Dynamical model of rocket propellant loading with liquid hydrogen. J Spacecr Rockets. 48(6):987–998. doi: 10.2514/1.52587

OSTI.GOV. 1993. Handbook of chemical hazard analysis procedures Tech. Rep. 6645955, Washington (DC): Federal Emergency Management Agency.

Petitpas G. 2018. Simulation of boil-off losses during transfer at a LH2 based hydrogen refueling station. Int J Hydrogen Energy. 43(46):21451–21463. doi: 10.1016/j.ijhydene.2018.09.132

Solomon S, Qin D, Manning, M, Chen Z, Marquis M, Averyt KB, Tignor M, Miller HL, editors. 2007. Contribution of working group I to the fourth assessment report of the intergovernmental panel on climate change. In: Climate change 2007: the physical science basis. Cambridge, United Kingdom and New York, NY, USA: Cambridge University Press; p. 996. IPCC.

Tryggvason G, Lu J. 2015. Direct numerical simulations of flows with phase change. Procedia IUTAM. 15:2–13. doi: 10.1016/j.piutam.2015.04.002

United Nations, G. A.. 2022. The sustainable development goals report.

Wang Z, Sharafian A, Mérida W. 2020. Non-equilibrium thermodynamic model for liquefied natural gas storage tanks. Energy. 190:116412. doi: 10.1016/j.energy.2019.116412

Welch S, Wilson J. 2000. A volume of fluid based method for fluid flows with phase change. J Comput Phys. 160(2):662–682. doi: 10.1006/jcph.2000.6481

Yang Z, Peng X, Ye P. 2008. Numerical and experimental investigation of two phase flow during boiling in a coiled tube. Int J Heat Mass Transf. 51(5):1003–1016. doi: 10.1016/j.ijheatmasstransfer.2007.05.025